



Thermal modeling for breast tumor detection using thermography

O. Mukhmetov^a, D. Igali^a, A. Mashekova^a, Y. Zhao^{a,*}, E.Y.K. Ng^b, S.C. Fok^a, S.L. Teh^a

^a Department of Mechanical and Aerospace Engineering, School of Engineering and Digital Sciences, Nazarbayev University, Nur-Sultan, 010000, Kazakhstan

^b School of Mechanical and Production Engineering, Nanyang Technological University, 50 Nanyang Avenue, 639798, Singapore

ARTICLE INFO

Keywords:

Finite element modelling
Breast cancer
Thermography
Thermal modelling

ABSTRACT

The paper aims to complement thermography with numerical analysis in order to use patients' personalized data such as precise breast geometry and temperature patterns to detect tumors inside the breast. Previous studies in the literature use idealized semi-spherical breast models without experimental validation and personalized data. To improve the accuracy and reliability of computer-aided diagnosis of breast tumors, this study uses realistic 3D breast geometry, based on 3D scanning, in its numerical model, which is then validated by experiments through fabricating the breast using 3D printing and molding. It is shown in the combined numerical and experimental study that breast geometry is very important in determining the temperature field and detecting the tumor inside the breast. Further computational study shows that for breasts with and without tumors for cup sizes ranging from 120 to 260 mm and tumor depth from 5 to 25 mm, the maximum differences in surface temperatures can range from 0.34 to 1.37 °C. The difference become insignificant with large cup sizes. Thus, it can be concluded that the major important factors for precision tumor detection are tumor depth and breast geometry.

1. Introduction

Breast cancer is the leading disease among women in terms of occurrence and fatality rate [1]. There are many techniques for the detection of breast cancer. Among them mammography is considered as the gold standard [2]. Nevertheless, one of the main disadvantage of this method is harmful ionizing radiation [3] as well as the difficulties to define the tumor inside of the dense breast [4]. Furthermore, in some countries mammography as a screening technique is only used for women over 30 years [5].

One of the approaches that is noninvasive, relatively cheap and based on investigating the temperature profile on the breast surface is thermography. The fundamentals of thermography are based on the constant human skin emissivity of 0.98 and the measurement of infrared radiation emitted from the objects with temperature above absolute zero. These allow the determination of the temperature profile of the skin surface through measurement of the infrared radiation emitted from the human [6,7].

There are many applications of infrared thermography in different medical diagnosis [7]. These areas of medical applications include the treatment of diabetes [8]; detection of seasonal influenza [9,10]; investigating of eye diseases [11]; screening modality for carotid artery stenosis [12]; analysis of chronic pain [13]; and the diagnosis of cancer

[14,15]. Infrared thermography is able to detect growing tumor because cancer cells have higher metabolic rate and thus heat generation rate than normal cells. According to Mital and Pidaparti [16], tumors with sizes varying from 5 to 15 mm, will have metabolic heat generation of 14,000 W/m³ to 70,000 W/m³ (Table 1).

Studies conducted by Satish et al. [17], Ng et al. [18], Gautheria et al. [19], Yahara et al. [20], and Ng [21] have shown that thermography is not only safe for pregnant women, but also effective for young women with dense breasts. It is recommended as a cheap technology to determine early symptoms of breast cancer. Based on the researches of Perisky et al. [22] and Keyserlingk [23], thermography can have sensitivity of 97% and specificity 83%. Recently there are interests to connect thermography with numerical analysis, data mining and image processing. Scientists envisage that the effectiveness of the thermography-based diagnosis could be improved by the use of these modern technologies such as finite element modelling, artificial intelligence [14], and machine learning.

This paper investigates the use of numerical analysis to complement thermography for the detection of breast tumor. The study consists of two parts. The first part involves the experimental study of the temperature profiles on the surface of a silicon breast with an artificial tumor using an infrared camera. The second part investigates the effect of heat generated in the artificial breast on the surface temperature

* Corresponding author. Nazarbayev University, 53 Kabanbay batyr avenue, Nur-Sultan, 010000, Kazakhstan.

E-mail address: yong.zhao@nu.edu.kz (Y. Zhao).

Table 1

Tumor metabolic heat generation.

Tumor diameter (mm)	4	8	12	15
Metabolic heat generation (W/m ³)	9818	25,000	40,000	70,000

**Fig. 1.** Breast region with targets.

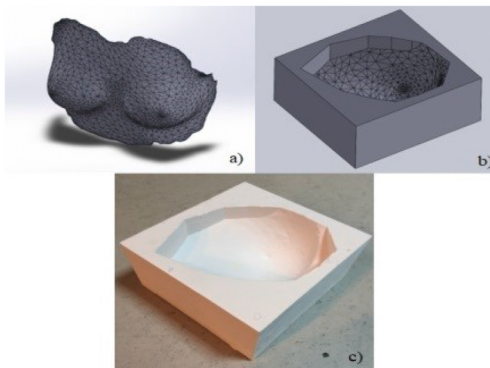
profiles with finite element analysis software (ANSYS 16.2). This work considered different factors such as breast cup size, tumor size and location in the breast. The experimental results were used to validate the finite element model. Through this work, the effects of the tumor properties with different breast sizes on the breast surface temperature profiles can be investigated. The results would be useful in the improvement of thermography-based breast cancer detection.

2. Materials and method of the experiment

2.1. Experiment design

ZScanner700 was employed to derive the 3D geometry of the breast. The breast of a mannequin with 800 mm height, 838 mm chest and 635 mm waist was used (Fig. 1). The positioning markers were randomly affixed on the mannequin's breast with a distance of 30 mm among them (Fig. 1). The markers were required for system position in 3D space. After 3D breast geometry was obtained, the point cloud data is converted automatically into an STL file in order to use for 3D printing of the mold and for the numerical study.

A 3D printer - ZPrinter 450 was used to print the mold (Fig. 2), which then was employed for breast casting (Fig. 3). For this purpose

**Fig. 2.** Mold printing: (a) scanned image by ZScanner 700; (b) 3D image of the mold created in Solidworks; (c) Mold manufactured by the 3D printer.**Table 2**

Heat source location and size.

Breast sample number as in Fig. 4(a-d)	1	2	3	4
Heat source location (mm)	x y z	92 89 35	95 100 54	145 80 40
The total number of resistors used	4	8	6	4
Total volume of the heat sources, mm ³	75.4	150.8	113.1	75.4

**Fig. 3.** Silicone Breasts with different locations: (a) with a tumor size of 75.4 mm³; (b) with a tumor size of 150.8 mm³; (c) with a tumor size of 113.1 mm³; (d) with a tumor size of 75.4 mm³

the Dragon Skin 10 MEDIUM Set Silicone Rubber was explored. This material is usually used to simulate the skin of the human body. The mold was filled with the liquid silicone and left to cure at room temperature for 4–6 h, after which the prepared silicone breast was released from the mold (Fig. 3).

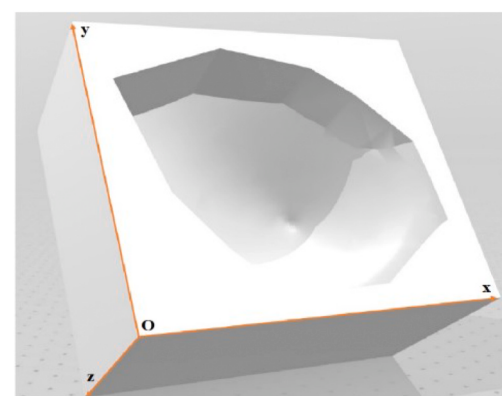
The heat sources made of resistors and wires were used as the tumors. Location of the tumors were preliminary defined and measured (Table 2) according to pre-defined X, Y, Z coordinates (Fig. 4).

Table 2 presents the location of the tumor in respect of X, Y, Z coordinates, as well as the number of the resistors used for the tumor simulation. Number of the resistors defines the amount of heat generated by the resistors, in other words number of the resistors defines the size of the tumor. Resistors have the length of 6 mm and diameter of 2 mm, whereas the volume of a resistor can be calculated as:

$$V = \pi r^2 h = \pi \times 1^2 \times 6 = 18.9 \text{ mm}^3$$

The total volume of the tumor is determined by multiplying the volume of one resistor by the total number of resistors used (Table 2).

In the experiments, a thermographic camera Fluke Ti29 was used to observe the temperature variations on the surfaces of the silicone breasts. In addition, Fluke Ti29 has IT-fusion technology and blend modes which allow the display and storage of full visual images (640 ×

**Fig. 4.** The pre-defined X,Y,Z axis of the coordinate system.

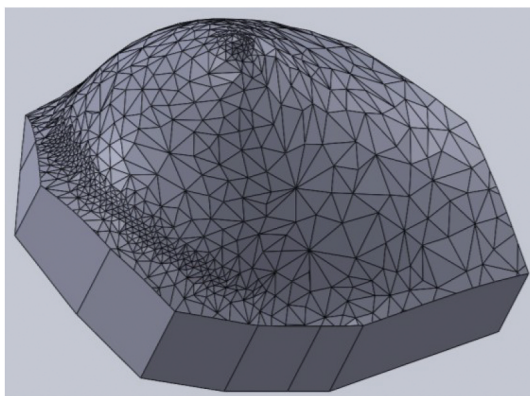


Fig. 5. 3D scanned and modified in SolidWorks model used for simulation study.

480) and thermal images simultaneously. These images can be transferred to a PC.

The infrared camera captured the temperature profiles of a silicone breast every 15 min. The temperature of the room was maintained at 24–26 °C, the initial breast temperature is assumed equal to the temperature of the desk.

2.2. Mathematical modelling

The mathematical model includes 3D geometrical model of the breast, the heat conduction equation and the numerical method (FEM) for its numerical solution, the initial and boundary conditions. As it was aforementioned, 3D geometry of the breast was obtained during scanning of the mannequin, therefore the obtained geometry was very closed to the geometry of the real breast.

Numerical model was based on solving of bio-heat Pennes' equation. Equation (1) shows the Pennes' equation [24]:

$$\rho c \frac{dT}{dt} = \nabla \cdot (k \nabla T) + \rho_b w_b c_b (T_a - T) + q_m \quad (1)$$

where T (K) is the temperature of the tissue equals to 297 K or 24 °C; ρ is the density (kg/m^3) and it equals to $1050 \text{ kg}/\text{m}^3$; c is the specific heat ($\text{J}/\text{kg}\cdot\text{K}$) equals to 3770 ($\text{J}/\text{kg}\cdot\text{K}$), k is the thermal conductivity of the tissue ($\text{W}/\text{m}\cdot\text{K}$) equals to 0.42 ($\text{W}/\text{m}\cdot\text{K}$). c_b is the specific heat of blood ($\text{J}/\text{kg}\cdot\text{K}$), which is in terms of the current research, is equal to zero, as the conducted experiments are based on the artificial homogenous breast without considering the blood flow. q_m is the metabolic heat generation per unit volume (W/m^3), which is in case of the current research is defined by the size of the tumor (Table 1). T_a represents the temperature of arterial blood (K) and equal to 310 K, the same as the core temperature of the body. In the research the temperature does not change with time, in other words it is steady-state condition, therefore the left hand side part of the equation equals to zero [26]:

$$k \nabla^2 T + \rho_b w_b (T_a - T) + q_m = 0 \quad (2)$$

Boundary conditions of the numerical modelling includes heat

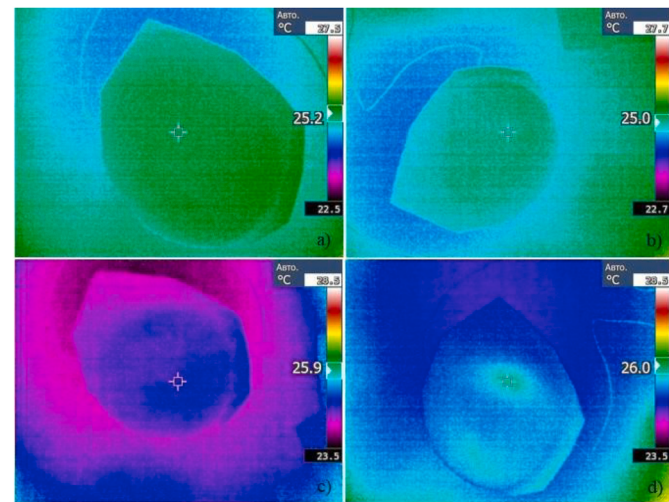


Fig. 6. Infrared image at every 15 min: (a) $P = 0.0027 \text{ W}$; (b) $P = 0.01608 \text{ W}$; (c) $P = 0.064 \text{ W}$; (d) $P = 0.25408 \text{ W}$. Tumor size 75.4 mm^3 with depth 35 mm.

Table 4

Recorded power outputs and maximum surface temperatures in experiment 1.

Measurement No.	Voltage, V	Current, A	Power Output, W	Temperature, °C
1	0	0	0	25.1
2	0.90	0.003	0.00270	25.2
3	2.01	0.008	0.01608	25.0
4	4.00	0.016	0.06400	25.9
5	7.94	0.032	0.25408	26.0

convection and the constant temperature, as follows:

$$-k \nabla T = h(T_s - T_a) \quad (3)$$

$$T = T_a \quad (4)$$

where h ($\text{W}/\text{m}^2 \cdot ^\circ\text{C}$) is convective heat transfer coefficient; T_s is the surface temperature; T_a is the ambient temperature equal to 24 °C. In addition, the skin temperature was also considered at 24 °C, as the experiments are conducted without clothing in a constant temperature and control environment.

Heat transfer coefficient is defined by experiments, so the conducted experiments [26–30] show that at temperatures from 20 °C to 30 °C the body losses heat by insensible evaporation. Taking this into consideration the integration of the mass equation due to loss of water from the body phase change is required. On the other hand, with aim of escaping such intricacy to equation (1) or (2), the thermographic measurements should be conducted under the strict protocol, and heat loss due to evaporation may be considered negligible. Thus, Osman and Afify in Refs. [27–29], assumed the heat transfer coefficient, h , equal to 13.5 $\text{W}/\text{m}^2 \cdot ^\circ\text{C}$.

As numerical solver for the bio-heat equation Finite Element Modelling was used. Taking into account equations (2) and (3) finite element model can be obtained as follows:

Table 3

Temperature probes positions and mesh verification study with four meshes/simulations.

	Coordinates (mm)			Temperature (K)			
	X	Y	z	Breast No. 1	Breast No. 2	Breast No. 3	Breast No. 4
Probe 1	100	95	-56.77	298.37	298.37	298.37	298.37
Probe 2	100	95	-25.23	298.65	298.65	298.65	298.65
Probe 3	110	95	41	298.67	298.67	298.67	298.67
No. of nodes				120,071	246,679	1,217,332	3,331,157
No. of elements				40,052	75,813	356,437	957,479

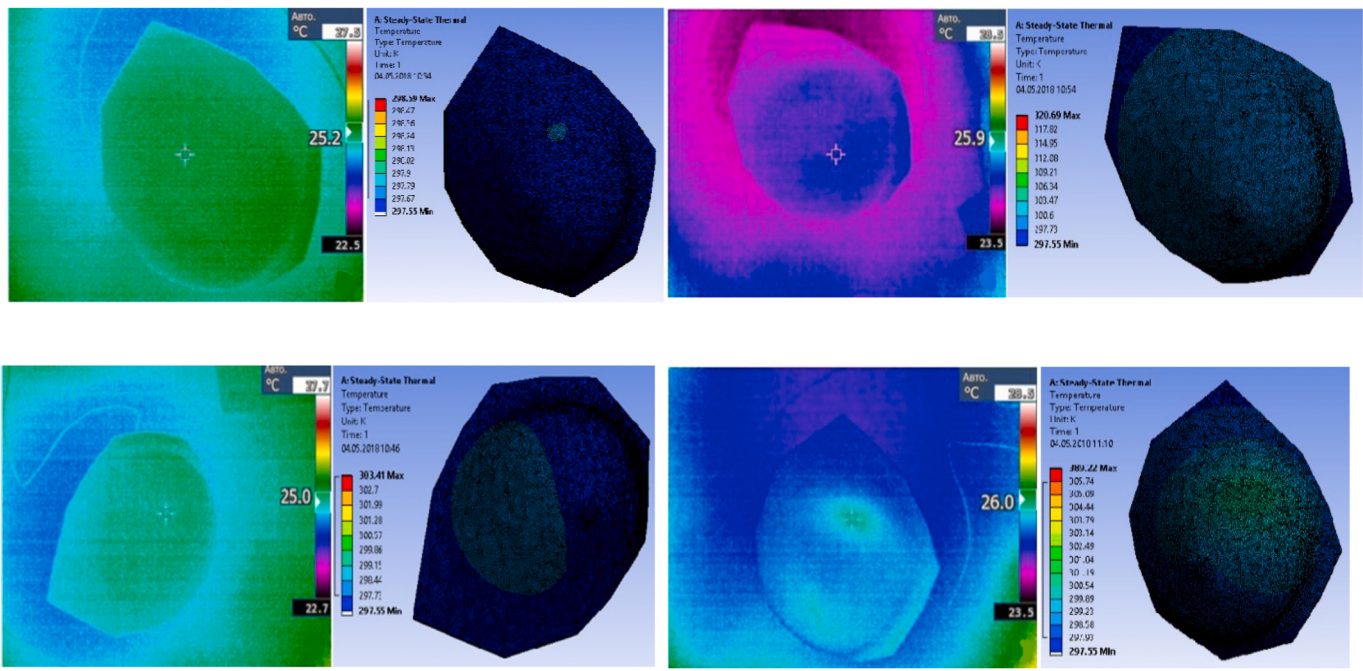


Fig. 7. Comparison of computed and experimental surface temperature profile at different powers for experiment 1.

Table 5
Simulation and experimental results for experiment 1.

Power (W)	Simulated Temperature (°C)	Experimental temperature (°C)	Error (%)	RMS Error (%)
0.00270	24.650	25.2	2.18	2.22
0.01608	24.700	25.0	1.20	
0.06400	24.881	25.9	3.93	
0.25408	25.597	26.0	1.55	

Table 6
Recorded power outputs and maximum temperatures in experiment 2.

Measurement No.	Voltage, V	Current, A	Power Output, W	Temperature, °C
1	0	0	0	25.6
2	1.62	0.005	0.0081	26.5
3	2.50	0.008	0.02	26.6
4	5.51	0.018	0.09918	26.7
5	8.55	0.027	0.23085	29.0

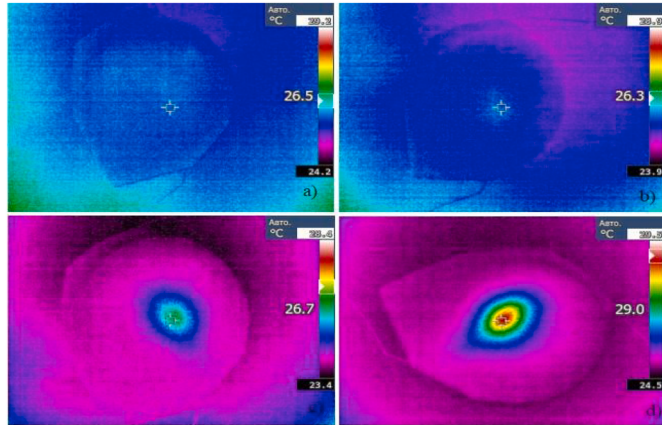


Fig. 8. Infrared image at every 15 min: (a) $P = 0.0081$ W; (b) $P = 0.02$ W; (c) $P = 0.09918$ W; (d) $P = 0.23085$ W. The tumor size 150.8 mm^3 with depth 54 mm.

$$\iiint_V k_x \frac{\partial W_1}{\partial x} \frac{\partial T}{\partial x} + k_y \frac{\partial W_1}{\partial y} \frac{\partial T}{\partial y} + k_z \frac{W_1}{\partial z} \frac{\partial T}{\partial z} - Q_m W_1 + \rho c \frac{\partial T}{\partial t} W_1 \Big) dv + \oint_S h_c (T - T_e) W_1 ds = 0 \quad (5)$$

where V is the volume integral range, S is surface integral range, w_1 is the weighting function.

The following steps should be taken in order to find numerical

solution: creating the 3D geometry model of the breast, meshing the geometry, defining tissue material thermal and physical properties, specifying the boundary conditions of the model, and finally numerically solve the governing equation for numerical solutions.

3D breast geometry used for the study is a unique feature of the research, which is a form of personalized data acquired by 3D scan, whose FEM mesh is shown in Fig. 5. The shape of the tumor imposed inside the breast has a circular and a spherical geometry. The characteristic of the tumor is the size, depth and location. With an aim to estimate these attributes of the tumor inside the breast, the skin surface temperature of the breast was analyzed.

Table 3 presents four simulations with three temperature probes with different mesh sizes. As a result of mesh verification study for further investigation, breast No. 3 (Table 3) was chosen, as the temperature differences between simulation studies No. 3 and 4 were less than 0.001 K.

In order to validate the numerical results by the experiment the same input data and constants were used. The size of the tumor, position of the

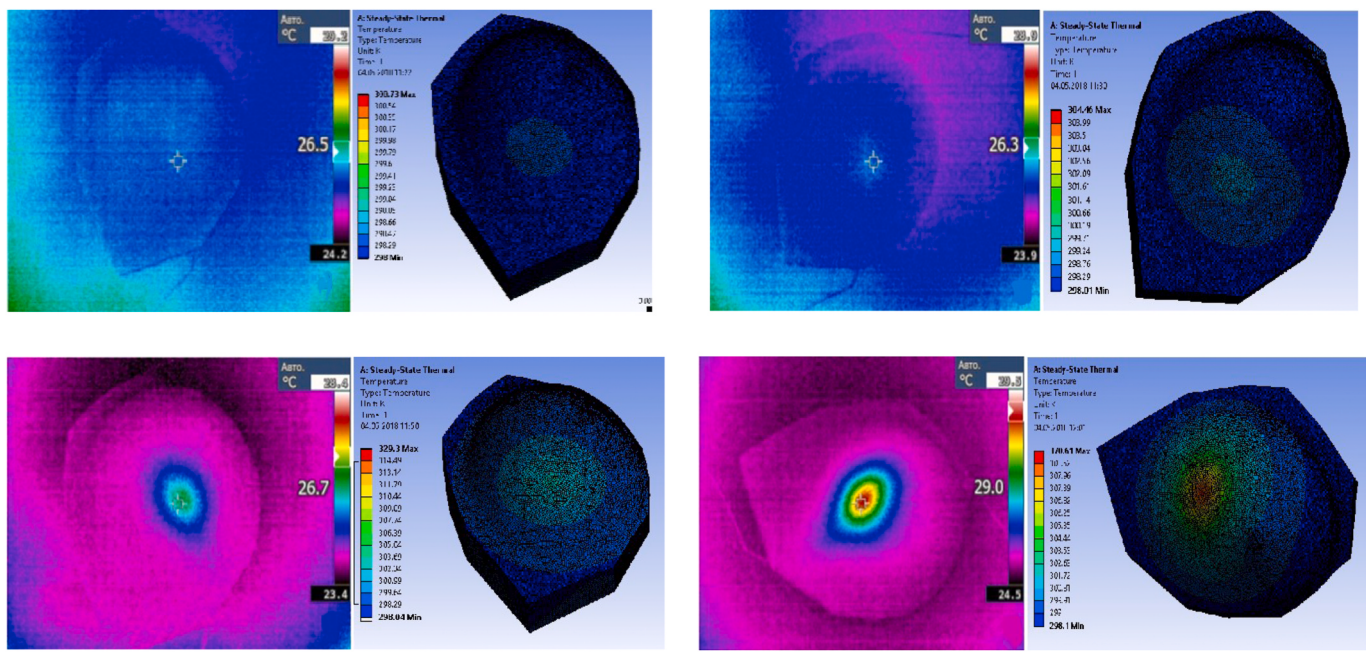


Fig. 9. Comparison of computed and experimental surface isotherms profile at different powers for experiment 2.

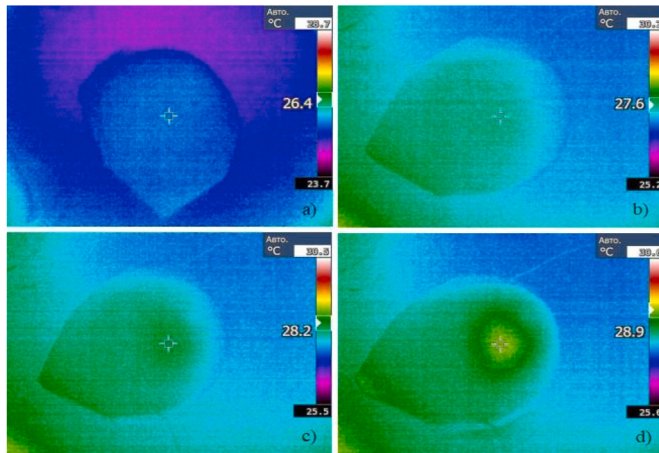


Fig. 10. Infrared image at every 15 min: (a) $P = 0.00486 \text{ W}$; (b) $P = 0.0459 \text{ W}$; (c) $P = 0.18685 \text{ W}$; (d) $P = 0.42224 \text{ W}$. The tumor size 113.1 mm^3 with depth 40 mm .

tumor, its heat generation rate, initial temperature, and ambient temperature used in the simulation were obtained from the experiments.

Thus, four experiments were conducted with four casted breasts. These experiments were modelled and simulated. The boundary condition used is the same in all simulation and was derived from the experimental conditions.

3. Results and discussion

The first experiment was performed on the silicone breast with a tumor size of 75.4 mm^3 . The room temperature was $24.5 \text{ }^\circ\text{C}$, and the desk temperature was $25.1 \text{ }^\circ\text{C}$. Fig. 6 presents the region with relatively hot temperature, that is located on top of the tumor and indicated by green color. The maximum voltage applied was 7.94 V and the corresponding power output was 0.25408 W . The maximum temperature on the breast surface was $26.0 \text{ }^\circ\text{C}$ (Table 4). Fig. 6 shows the maximum temperatures on the breast surface corresponding to changes in power outputs.

Table 8
Recorded power outputs and maximum surface temperatures in experiment 3.

No. of measures	Voltage, V	Current, A	Power Output, W	Temperature, $^\circ\text{C}$
1	0	0	0	26.3
2	0.81	0.006	0.00486	26.4
3	2.55	0.018	0.0459	27.6
4	5.05	0.037	0.18685	28.2
5	7.54	0.056	0.42224	28.9

Table 9
Simulation and experimental results for experiment 3.

Power (W)	Simulated Temperature ($^\circ\text{C}$)	Experimental Temperature ($^\circ\text{C}$)	Error (%)	RMS (%)
0.00486	26.464	26.4	0.24	2.72
0.0459	26.750	27.6	3.08	
0.18685	27.051	28.2	4.08	
0.42224	27.751	28.9	3.97	

Simulation of the first experiment was performed using the associated data for the tumor size, position, heat generation rate, initial and ambient temperatures. Fig. 7 compares the computed and experimental temperature (isotherms) profiles. Table 5 tabulates the maximum experimental and simulated temperatures at various power levels. It can be seen that as the power level increases, the maximum temperature also increases. This is due to the increase in heat release rate (HRR) which in turn increases the size of hot region on the breast surface.

The second experiment was performed on the silicone breast with tumor size of 150.8 mm^3 . The room temperature was $24.8 \text{ }^\circ\text{C}$, and the desk temperature was $25.6 \text{ }^\circ\text{C}$. From Fig. 8 it can be seen, that the hottest region is located on the top of the tumor and indicated by red color. In this case, the presence of the tumor is very clear, since it is located close to the breast surface. The location of the tumor could be described by the coordinates $x = 95 \text{ mm}$, $y = 100 \text{ mm}$, $z = 54 \text{ mm}$.

The values of the given voltage, current and measured maximum temperature are provided in Table 6.

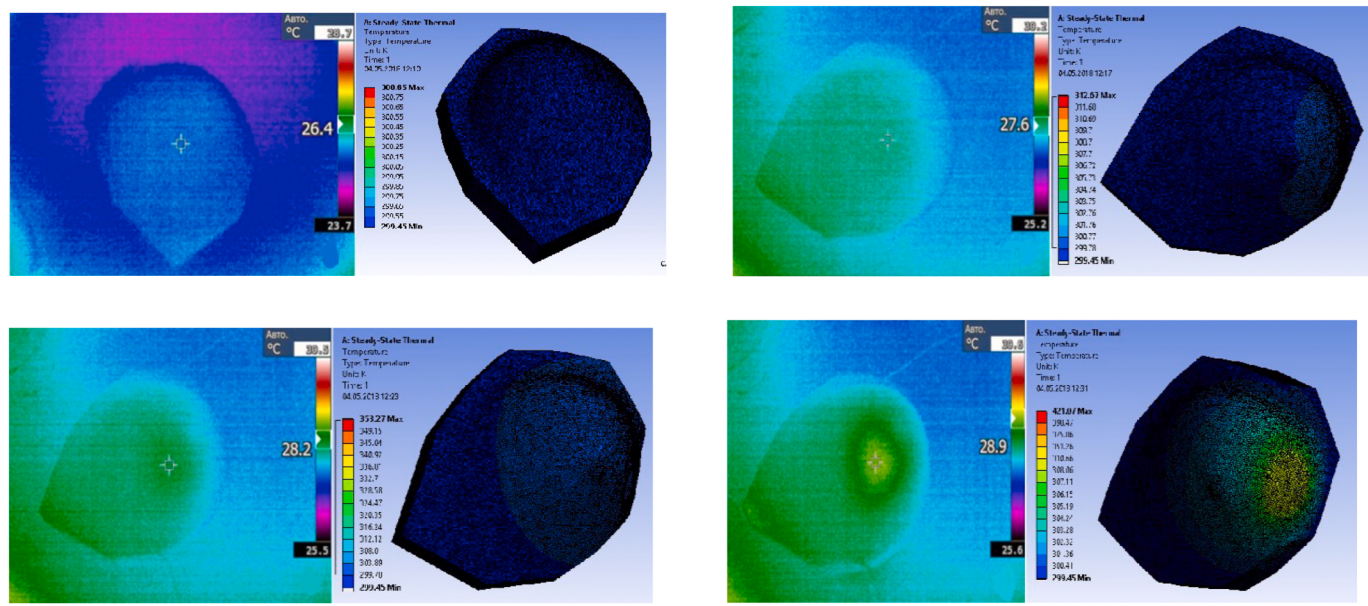


Fig. 11. Comparison of computed and experimental surface isotherms profile at different powers for experiment 3.

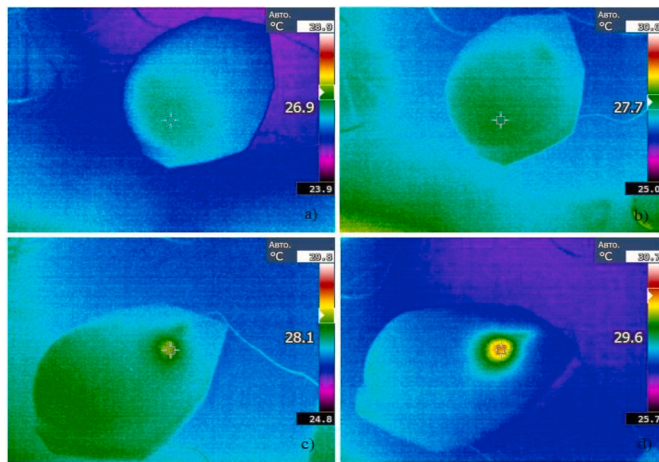


Fig. 12. Infrared image at every 15 min: (a) $P = 0.00297$ W; (b) $P = 0.01592$ W; (c) $P = 0.05012$ W; (d) $P = 0.16848$ W. Tumor size 75.4 mm^3 with depth 45 mm.

In experiment 1, there was a drop in temperature from 25.2 °C to 25.0 °C as the power increased from 0.0027 W to 0.01608 W. In experiment 2, there was a drop in temperature from 26.5 °C to 26.3 °C as the power increased from 0.0081 W to 0.02 W. The results indicated that at low power, some discrepancies could exist in the thermography results, as the convection heat loss faster than the heat source generation or at least in the similar order of magnitude. At higher power, the trend is clear and the discrepancies become insignificant.

Table 7 tabulates the maximum experimental and simulated temperatures at various power levels for experiment 2 while Fig. 9 compares the simulated and experimental thermograms. The root means square (RMS) error for experiment 2 was 3.23%.

The third experiment was performed on the silicone breast with the tumor size of 113.1 mm^3 . The room and desk temperature are 24.6 °C and 25.5 °C, respectively. In this case, there is only rising trend without any temperature drop.

The region with relatively hot temperature was located exactly on the top of the tumor and indicated by light green color in Fig. 10. The maximum voltage supplied to the resistors was equal to 7.54 V, with the

Table 10
Recorded power outputs and maximum surface temperatures in experiment 4.

No. of measures	Voltage, V	Current, A	Power Output, W	Temperature, °C
1	0	0	0	26.1
2	0.99	0.003	0.00297	26.9
3	1.99	0.008	0.01592	27.7
4	3.58	0.014	0.05012	28.1
5	6.48	0.026	0.16848	29.6

Table 11
Simulation and experimental results for Breast 4.

Power (W)	Simulated Temperature (°C)	Experimental Temperature (°C)	Error (%)	RMS (%)
0.00297	26.261	26.9	2.38	0.66
0.01592	27.493	27.7	0.75	
0.05012	28.194	28.1	0.34	
0.16848	29.645	29.6	0.15	

corresponding power output equal to 0.42224 W. The maximum surface temperature was 28.9 °C (Table 8).

Fig. 11 shows the temperature contours obtained from simulation and IR imaging in experiment 3.

Table 9 compares the maximum surface isotherms with respect to output powers in experiment 3. The root means square error for experiment 3 was 2.72%.

The fourth experiment was performed on the silicone breast with the tumor size of 75.4 mm^3 . The room and desk temperature are 24.8 °C and 25.3 °C respectively. The region with relatively hot temperature is located exactly on the top of the tumor and indicated by red color in Fig. 12.

Table 10 presents the recorded power outputs and corresponding maximum isotherms in experiment 4. The maximum surface temperature at power output of 0.16848 W was 29.6 °C.

The RMS error for experiment 4 is tabulated in Table 11. Fig. 13 reveals the temperature profiles obtained from the simulation and experiment 4 results. In the four experiments, the RMS errors in average were 2.2%.

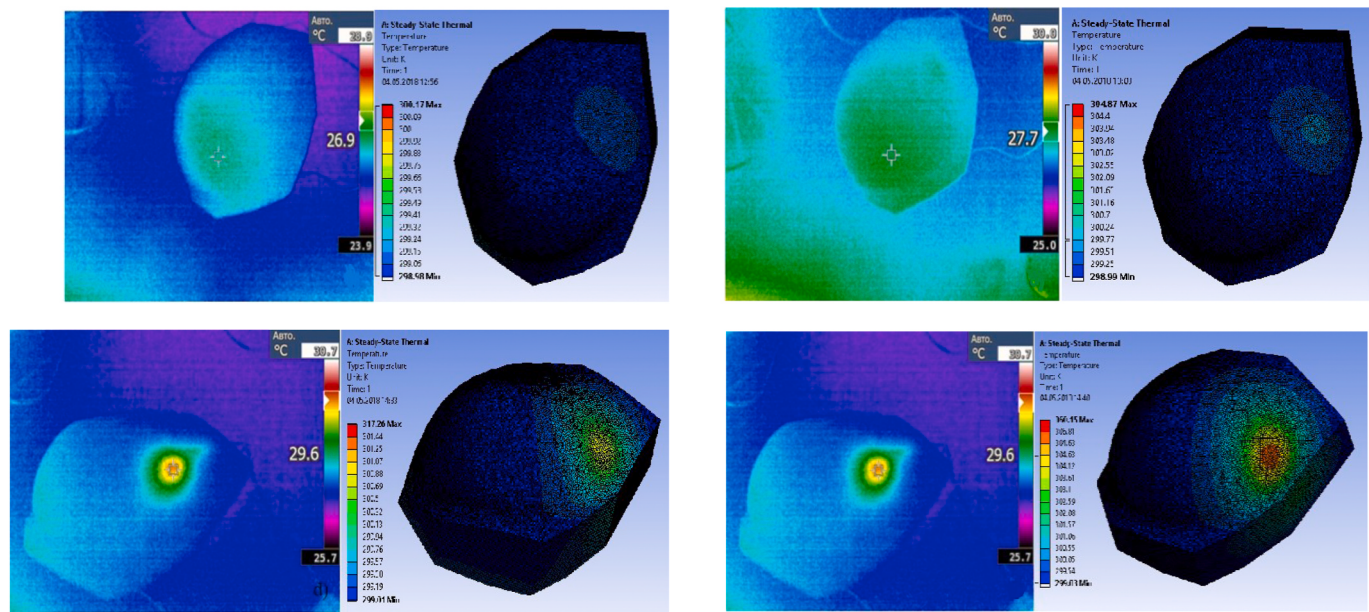


Fig. 13. Comparison of computed and experimental temperature profile at different powers for experiment 4.

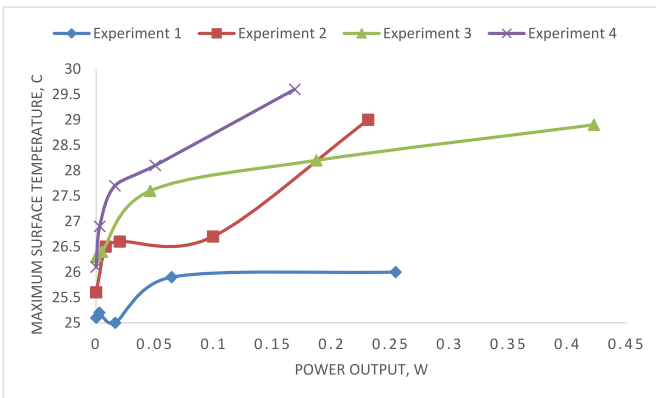


Fig. 14. Power output vs. maximum surface temperature.

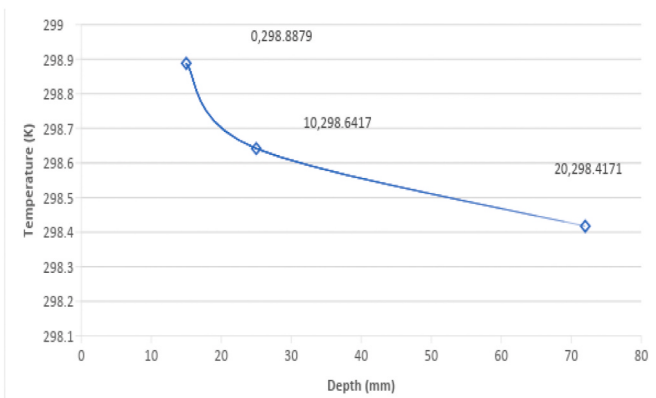


Fig. 15. Depth vs temperature on the nipple.

Fig. 14 shows the power output versus maximum surface temperatures for the four experiments. In experiment 1, the change in maximum temperature with increasing power output is almost constant after 0.1 W. In experiment 3, there is a graduate increase in

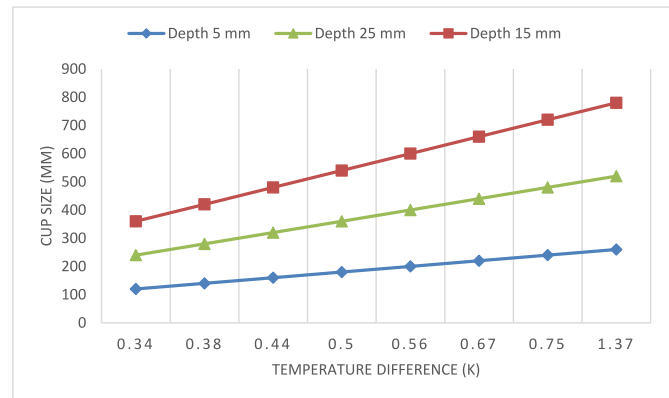


Fig. 16. Temperature difference vs cup size, at different depth.

maximum temperature with increasing power output. Experiments 2 and 4 show more significant increase in maximum temperature with increasing power output. The tumors in experiments 2 and 4 are located near to the breast surface and this could contribute to rapid increase in maximum temperature with increasing output power. In experiments 1 and 3, the tumors are located deeper inside the breast. As such it can be envisaged that the location of the tumor can affect the gradient of the curve in **Fig. 14** [31]. Convection on the breast surface which is dependent on the ambient (and desk) temperature and initial temperature of the breast, could be a factor in the determination of the gradients in the curves of **Fig. 14** [32].

Thus, comparison of the computed results and the experimental data shows that the RMS percentage error deviates from 0.66% to 3.23%. This is an acceptable error range and suggests good correlation between the simulated and experimental results. The errors could be due to the variation in convection heat transfer during the experiment. In addition, the uncertainties of the resistors are unknown and could affect the heat dissipation.

After validation of the mathematical and experimental results, additional simulations were conducted on the effects of cup size, tumor size and depth on the surface temperature. The results of tumor depth on the surface temperature are shown in **Fig. 15**. The findings indicated that the deeper the tumor inside the breast, the lower is the surface

temperature. However, the decrease in temperature is very small, as the heat generation between the tumor size are also small [31,32].

Fig. 16 shows the temperature differences between breast with and without tumor versus cup size at different tumor depths. It is clear, that at the same cup size, the temperature differences between a breast with and without tumor decreases as the tumor depth increases. For breasts with and without tumors for cup sizes ranging from 120 to 260 mm and tumor depth ranging from 5 to 25 mm, the maximum differences in surface temperatures can range from 0.34 to 1.37 °C. The differences become insignificant with large cup size. At cup size of 260 mm, the temperature differences will not be able to distinguish the tumor depths. These simulation findings indicated that the location of the tumor and the breast geometry affects the temperature distribution on the breast surface. This assumption is also supported by other research studies which concluded that depth of the tumor and size of the breast is the most important factor among all other features such as size of the tumor, size of the breast or location of the tumor.

4. Conclusion

A novel framework of experimental and computational procedures has been successfully developed, which uses artificial breasts based on 3D scanning and 3D printing and molding to validate accurate numerical breast models for the purpose of precision diagnosis of breast cancer employing personalized data, such as scanned 3D breast geometry and thermograms. The framework and the models thus developed and validated can be extremely useful for fast and precision diagnosis of breast cancer using inverse thermal modelling techniques. Detailed experiments on artificial breasts were conducted and experimental measurements were used to validate the FEM breast models with simulated tumors. The combined experimental and numerical study does prove that the tumor inside the breast can give different temperature profiles depending on geometrical conditions, such as the location, depth and size of the tumor, as well as the breast geometry and size. Therefore, it is revealed with solid evident that personalized data, such as patients' breast 3D geometry and tumor size, play important roles in precision computer-aided diagnosis of breast cancer, which have largely been ignored in past studies.

Furthermore, this study shows that the RMS percentage error of the FEM results ranges from 0.66% to 3.23%, which proves that FEM can be used for precision tumor diagnosis. This is important as the development of finite-element-based inverse thermal modelling could improve the performance of thermography-based breast cancer detection. Through their integration, thermography can be better established as a suitable, non-invasive, easy to use and cheap technique for early breast cancer detection. The accuracy of models developed can be further enhanced by incorporating a numerical procedure to extract more personalized data in the form of tissue mechanical properties, such as density, thermal conductivity and fat content of the breast, which will, however, slow down the speed of diagnosis.

Declaration of competing interest

The authors declare that they have no known competing financial interests or personal relationships that could have appeared to influence the work reported in this paper.

Data availability

No data was used for the research described in the article.

Acknowledgement

The authors are grateful to Ministry of Education and Science of the Republic of Kazakhstan for financing this work through the grant for the "Development of an intelligent system for early breast tumor

detection and cancer prediction" (AP05130923) and Nazarbayev University Research and Innovation System for administrating the research project.

References

- [1] L. Peng, W. Chen, W. Zhou, F. Li, J. Yang, J. Zhang, An immune-inspired semi supervised algorithm for breast cancer diagnosis, *Comput. Methods Progr. Biomed.* 134 (2016) 259–265.
- [2] M.C. Araujo, R.C. Lima, R.M. De Souza, Interval symbolic feature extraction for thermography breast cancer detection, *Expert Syst. Appl.* 41 (2014) 6728–6737.
- [3] S.V. Francis, M. Sasikala, G.B. Bharathi, S.D. Jaiparkar, Breast cancer detection in rotational thermography images using texture features, *Infrared Phys. Technol.* 67 (2014) 490–496.
- [4] E. Gerasimova, B. Audit, S.G. Roux, A. Khalil, O. Gileva, E. Argoul, O. Naimark, A. Arneodo, Wavelet-based multifractal analysis of dynamic infrared thermograms to assist in early breast cancer diagnosis, *Front. Physiol.* 5 (2014) 176.
- [5] U.S. Preventive Services Task Force, Screening for breast cancer: U.S. Preventive services task force recommendation statement, *Ann. Intern. Med.* 151 (2009) 716–726.
- [6] N.A. Diakides, Bronzino J.D. *Medical Infrared Imaging*, CRC Press, Boca Raton FL, 2008.
- [7] I. Fernandez-Cuevas, J.C.B. Marins, J.A. Lastras, P.M.G. Carmona, S.P. Cano, M. A. Garcia-Concepcion, M. Sillero-Quintana, Classification of factors influencing the use of infrared thermography in humans: a review, *Infrared Phys. Technol.* 71 (2015) 28–55.
- [8] F. Ring, Thermal imaging today and its relevance to diabetes, *J. Diabetes Sci. Technol.* 4 (2010) 857–862.
- [9] G. Sun, T. Saga, T. Shimizu, Y. Hakozaiki, T. Matsui, Fever screening of seasonal influenza patients using a cost effective thermopile array with small pixels for close-range thermometry, *Int. J. Infect. Dis.* 25 (2014) 56–58.
- [10] E.Y.-K. Ng, Is thermal scanner losing its bite in mass screening of fever due to SARS? *Med. Phys.* 32 (1) (2005) 93–97.
- [11] J.H. Tan, E.Y.K. Ng, U.R. Acharya, C. Chee, Infrared thermography on ocular surface temperature: a review, *Infrared Phys. Technol.* 52 (2009) 97–108.
- [12] A. Saxena, E.Y.-K. Ng, S.T. Lim, Infrared thermography as a potential screening modality for carotid artery stenosis, *Comput. Biol. Med.* 113 (2019), <https://doi.org/10.1016/j.combiomed.2019.103419>.
- [13] J. Jarrell, C. Spanswick, Diagnostic use of infrared thermography in a patient with chronic pain following electrocution: a case report, *J. Med. Case Rep.* 3 (2009), <https://doi.org/10.4076/1752-1947-3-8992>.
- [14] U. Raghavendra, A. Gudigara, T.N. Rao, E.J. Ciaccio, E.Y.-K. Ng, U.R. Acharya, Computer aided diagnosis for the identification of breast cancer using thermogram images: a comprehensive review, *Infrared Phys. Technol.* 102 (2019) 103041, <https://doi.org/10.1016/j.infrared.2019.103041>.
- [15] R. Lawson, Implications of surface temperatures in the diagnosis of breast cancer, *Can. Med. Assoc. J.* 75 (1956) 309–310.
- [16] M. Mital, R.M. Pidaparti, Breast tumor simulation and parameters estimation using evolutionary algorithms, *Model. Simulat. Eng.* (1–4) (2008) 4.
- [17] Satish G. Kandlikar, Isaac Perez-Raya, Pruthvik A. Raghupathi, Jose-Luis Gonzalez-Hernandez, Donnette Dabydeen, Lori Medeiros, Pradyumna Phatak, Infrared imaging technology for breast cancer detection – current status, protocols and new directions, *Int. J. Heat Mass Tran.* 108 (2017) 2303–2320.
- [18] A. Saxena, E.Y.-K. Ng, V. Raman, M. Syarifuddin, M. Moderhak, S. Kolacz, J. Jankau, Infrared thermography-based quantitative parameters to predict the risk of post-operative cancerous breast resection flap necrosis, *Infrared Phys. Technol.* 103 (2019) 103063, <https://doi.org/10.1016/j.infrared.2019.103063>.
- [19] M. Gautheria, C.M. Gros, Breast thermography and cancer risk prediction, *Cancer* 45 (1980) 51–56.
- [20] T. Yahara, T. Koga, S. Yoshida, S. Nakagawa, H. Deguchi, and K. Shirouzu, Relationship between microvessel density and thermographic hot areas in breast cancer, *surg. Today Off.*, vol. 33, no. 4, pp. 243–248.
- [21] E.Y.-K. Ng, A review of thermography as promising non-invasive detection modality for breast tumour, *Int. J. Therm. Sci.* 48 (5) (2009) 849–855, <https://doi.org/10.1016/j.ijthermalsci.2008.06.015>.
- [22] Y.R. Parisky, A. Sardi, R. Hamm, et al., Efficacy of computerized infrared imaging analysis to evaluate mammographically suspicious lesions, *AJR Am. J. Roentgenol.* 180 (2003) 263–269.
- [23] J.R. Keyserlingk, P.D. Ahlgren, E. Yu, N. Belliveau, M. Yassa, Functional infrared imaging of the breast, *IEEE Eng. Med. Biol.* 19 (2000) 30–41.
- [24] Engineers edge. (n.d.). Convection heat transfer coefficients table chart. http://www.engineersedge.com/heat_transfer/conductive_heat_transfer_coefficient_s_13378.htm (Accessed October 2019).
- [25] M. Ghassemi, A. Shahidian, *Nano and Bio Heat Transfer and Fluid Flow*, Elsevier Academic Press, UK, 2017, p. 145.
- [26] M.M. Osman, E.M. Afify, Thermal modelling of the normal woman's breast, *Trans. ASME, J. Biomech. Engng* 106 (1984) 123–130.
- [27] E.Y.-K. Ng, N.M. Sudharsan, An improved three-dimensional direct numerical modelling and thermal analysis of a female breast with tumour, *Proc. IME H J. Eng. Med.* 215 (1) (2001) 25–37.
- [28] E.Y.-K. Ng, N.M. Sudharsan, Computer simulation in conjunction with medical thermography as an adjunct tool for early detection of breast cancer, *BMC Canc.* 4 (17) (2004) 1–26. <http://www.biomedcentral.com/1471-2407/4/17>.

- [30] E.Y.-K. Ng, N.M. Sudharsan, Effect of blood flow, tumour and cold stress in a female breast: a novel time-accurate computer simulation, Proc. Inst. Mech. Eng. 215 (H4) (2001) 393–404.
- [31] N.M. Sudharsan, E.Y.-K. Ng, Parametric optimisation for tumour identification: bioheat equation using ANOVA & taguchi method, International Journal of Engineering in Medicine 214 (5) (2000) 505–512.
- [32] N.M. Sudharsan, E.Y.-K. Ng, S.L. Teh, Surface temperature distribution of a breast with/without tumor, International Journal of Computer Methods in Biomechanics and Biomedical Engineering 2 (1999) 187–199.